UCRL-ID-143434

Hanford Science and Technology Program: Reaction Transport Experiments Investigating the Migration of 137Cs in Sediments beneath the Hanford SX Tank Farm

S. Carrol, C. Steefel, P. Zhao, and S. Roberts

U.S. Department of Energy
Lawrence Livermore National Laboratory

April 18, 2001

DISCLAIMER

This work was performed under the auspices of the U. S. Department of Energy by the University of California, Lawrence Livermore National Laboratory under Contract No. W-7405-Eng-48.

Hanford Science and Technology Program: Reaction Transport Experiments Investigating the Migration of ^{137}Cs in Sediments Beneath the Hanford SX Tank Farm

Susan Carroll, Carl Steefel, Pihong Zhao and Sarah Roberts
Lawrence Livermore National Laboratory

I. Introduction

Over one million gallons of high–level–waste with more than a million curies of ^{137}Cs have leaked from Hanford tank farms to the sediments beneath the tanks. Early on, it was assumed that cesium migration would be limited because laboratory experiments had shown that cesium strongly sorbs to phyllosilicate minerals common in soils [1-5]. Additionally, minimal cesium desorption has been observed in contaminated Hanford sediments [6]. However, recent observations beneath the Hanford tank farms show that cesium has migrated to greater depths than expected [7]. Various explanations for enhanced cesium migration include 1) physical processes such as fast flow pathways or bypassing of exchange sites in immobile zones, and 2) chemical processes associated with the very high salt contents and high pH of the tank fluids. Ion exchange processes are clearly indicated in the depth profiles of ^{137}Cs, and potassium, sodium, calcium, and nitrate (acting as a tracer) from the bore holes beneath tank SX-108 and tank SX-115. Below both tanks, cesium concentration peaks are retarded with respect to potassium and sodium concentration peaks. The importance of cation concentration on ion exchange is illustrated by comparing the sodium and tracer profiles beneath the tanks. Pore water with high sodium concentrations at SX-108 show little or no retardation of sodium, as is indicated by superimposed sodium and nitrate peaks. In contrast, at SX-115 sodium is significantly retarded relative to tracers (nitrate and Tc), presumably due to the lower sodium concentrations of the SX-115 leaks compared to SX-108 leaks. Calcium and magnesium form very distinct peaks at the leading edge of the sodium front under both SX-108 and SX-115. Observations such as these, led Zachara and his co-workers [8] to conduct a series of systematic cesium experiments over a wide range of cesium and salt concentrations to develop an ion exchange model that could be used to predict cesium migration beneath the Hanford tank farms.

We report reactive transport experiments of cesium sorption to Hanford sediments, with the specific objective of testing the applicability of cation exchange models derived from batch experiments to calculate cesium mobility beneath the Hanford tank farms. These experiments couple cesium exchange thermodynamics determined for Hanford sediments based on the batch experiments by Zachara and co-workers [8] and flow and transport using a reactive transport model [9]. Our experiments include (a) binary sodium–cesium exchange experiments at two different high salt and cesium concentrations, (b) a ternary potassium–sodium–cesium exchange experiment, and (c) a high base experiment in which mineral dissolution and precipitation affect cesium exchange. These experiments provide a more direct measure of retardation of cesium in Hanford sediments, which can be used in field-scale analyses of transport in addition to testing the applicability of the batch-derived exchange model. Our experiments investigate the reversibility of cesium exchange dominated by sorption to high affinity, frayed-edge sites on micas (FES sites) and to basal layers of expandable clay minerals (clay sites). Results of the high salt reactive transport experiments form the building blocks from which we determine the validity of extending the cesium exchange model to the very reactive tank wastes containing concentrated base solutions at elevated temperatures.

II. Experimental and Modeling Procedures

Experimental

A total of six one–dimensional column experiments using ground uncontaminated Hanford sediments were carried out in at 25°C to investigate the reactive transport of cesium (Table 1). We used the same Hanford formation composite sediments from RCRA monitoring wells surrounding the S-SX tank farm as were used in the batch experiments of Zachara et al [8]. Upon receiving these sediments they had already been lightly crushed to pass through a 2 mm sieve, air–dried and mixed thoroughly. No further fractionation of the sediments was conducted. The sediments were loaded into a reactor column (1.06 cm x 15.27 cm) filled with distilled and deionized water. Sediment density was determined to be 2.67 g cm^{-3} by

volume displacement. The reactive transport experiments consisted of three phases. In the pretreatment phase, the background electrolyte was passed through the column to replace potassium, calcium, and magnesium with sodium on the sediment exchange sites. Complete exchange was achieved in seven to ten pore volumes. The pretreatment phase of the experiment also provides an independent measure of the sediment cation exchange capacity (CEC). The pretreatment phase was followed by the cesium sorption experiment in which a CsI and $NaNO_3$ (or mixed KNO_3–$NaNO_3$, or NaOH) solution was passed through the sediment column to measure cesium retardation from the breakthrough curve. The final phase was a cesium desorption experiment in which the background electrolyte solution was passed through the sediment column to remove Cs from the exchange sites to assess the reversibility of the cation exchange reactions. Iodide behaved as a non-reactive tracer and was used to obtain a dispersivity of 1 cm. Aqueous samples exiting the column were analyzed for pH, Al, Ca, Cs, Fe, K, Mn, Mg, Na, and Si. The post-mortem sediments were examined by SEM/EDS and by X-ray diffraction for evidence of mineral reaction.

The sediment cation exchange capacity of the unreacted sediments and those reacted in 1 N NaOH were measured from triplicate ^{22}Na isotopic equilibrium experiments. Sodium saturated sediments were rinsed repeatedly with 2 mM $NaNO_3$ until a constant conductivity was reached to remove excess sodium from the sediment pore water. The dry, treated sediments were then reacted in 2 mM $NaNO_3$ spiked with ^{22}Na (10^5 dpm/ml ^{22}Na - $NaNO_3$) for 24 hours. After equilibration, the suspensions were centrifuged, and the supernatant was filtered and analyzed for ^{22}Na by liquid scintillation and total Na by ICP-AES. The sediment cation exchange capacity was also measured from the equivalent sum of Ca, K, Mg, and Na eluted with $NaNO_3$ and KNO_3 flushes of the sediments.

Table 1. One – Dimensional Cesium Reactive Transport Experiments

Exp. No.	Inlet Salt Solution	Inlet Cs M	Flow Rate (ml min^{-1})	Darcy Flux (cm min^{-1})	Sediment : Solution (g/L)	% Porosity
1	1 M $NaNO_3$	10^{-4}	0.1	0.025	3529.0	38.2
2	1 M $NaNO_3$	10^{-4}	0.02	0.113	3682.9	40.4
3	5 M $NaNO_3$	10^{-4}	0.1	0.121	3921.8	40.5
4	1 M NaOH	10^{-4}	0.02	0.023	4195.1	38.9
5	1 M $NaNO_3$	5×10^{-7}	0.1	0.113	3818.1	41.1
6	0.1 M KNO_3 0.9 M $NaNO_3$	10^{-4}	0.1	0.113	3483.5	43.4

Modeling

Modeling of cesium transport in the column experiments was carried out with the reactive transport code CRUNCH [9]. The code includes the capability for simulating multi-component ion exchange coupled to aqueous complexation and mineral precipitation and dissolution. Two sets of input were used to carry out the reactive transport simulations. One set of selectivity coefficients and exchange site concentrations were determined from a global fit of the all of Zachara et al's [8] batch Cs-Na, Cs-K, and Cs-Ca exchange experiments at background electrolyte concentrations of 5 M or less (Figure 1) (these are referred to as the "batch parameters"). The other set of selectivity coefficients and site concentrations was determined from batch and column experiments, strongly weighting of the column experiments in the optimization procedure (these are referred to as the "column parameters"). The fitting was carried out with the general fitting code PEST used in conjunction with speciation calculations carried out by CRUNCH. In this way, the resulting parameter set is fully compatible with the reactive transport simulations of cesium migration in both the column experiments and the field. Differences between the fits to the batch data presented here and those presented by Zachara et al [8] include activity coefficient corrections and aqueous complexation.

The selectivity coefficients in Table 2 were fit assuming the Gapon activity convention:

$$Cs^+ + M_{1/m}X \leftrightarrow CsX + {}^1\!/_m M \qquad 1.$$

where M is the exchanging cation (Na^+, K^+, Ca^{2+}) and m is its charge [10]. The exchange reactions can then be used to write a standard mass action equation for binary Cs-M exchange:

$$K_{M/Cs} = \frac{[M_{1/m}X][Cs^+]}{[CsX][M]^{1/m}} \qquad 2.$$

Multiple exchange sites were needed to capture the large range in the cesium K_d as a function of cesium concentration. The need for multiple sites with differing affinities can also be seen by plotting conditional equilibrium constants as was done by Zachara et al [8] who used a 2 site model to fit the data. Zachara et al [8] have presented the physical evidence for the existence of at least two sites with very different affinities for cesium, one associated with the frayed edges of micas and the other with the surfaces of clay particles. We have fitted cesium exchange with a three-site model because it provides a substantially better fit of the Cs-Ca and, to a lesser extent, the Cs-Na exchange data. The three-site model was used because of the improvement it gave in matching the batch data—there is no clear physical evidence for more than two distinct sites actually present in the Hanford sediments.

We chose to fit the cation exchange capacity (CEC) rather than using an independently determined value, because there is significant uncertainty in the CEC determined for these Hanford sediments. The highest CEC value was determined by cation elution during preliminary washes of the sediment (CEC = 138 μeq g^{-1}) [this study]. The next highest CEC value was determined by extraction of potassium by ammonium acetate (CEC = 83 μeq g^{-1}) [8]. The lowest CEC values were determined by ^{22}Na and ^{45}Ca isotopic equilibria measurements, (CEC = 46 ± 3 μeq g^{-1}) [8, this study]. Additional experiments are planned to help resolve the CEC so that it can be imposed as an independent constraint in the fitting of the exchange selectivity coefficients. The CEC of high affinity sites (as opposed to the total CEC) still needs to be fitted, however, since this cannot be determined with conventional CEC determinations. With the current model, the fits are non-unique as is shown by strong inverse correlation between selectivity coefficients for a particular site and the CEC of that site.

We used a standard Debye-Huckel formulation for activity coefficients augmented with fitting parameters for ion pair formation to describe solution activities accurately in the highly concentrated and variable Hanford system. Free cation activities were calculated by adjusting the log Ks for the ion pairs $CsNO_3(aq)$, $Ca(NO_3)_2(aq)$ and $NaNO_3(aq)$ to match ion activities determined with the Pitzer approach as implemented in the code GMIN [11]. It was also necessary to include an empirical activity coefficient correction for the various Cs exchange species in order to capture the ionic strength dependence of the exchange. This took the form of a standard "Bdot" correction in the extended Debye-Huckel equation:

$$\ln \gamma_{Cs-X} = BI \qquad 3.$$

Table 2. Cesium exchange selectivity coefficients, ion pair formation constants and CEC derived from a global fit to Zachara et al's [8] batch binary exchange experiments (Batch Parmeters) and derived from fits heavily weighted with column exchange experiments (Column Parameters).

Exchange Reaction	**Batch Parameters Log K**	**Column Parameters Log K**
$NaX1 + Cs^+ = Na^+ + CsX1$	6.96	6.85
$NaX2 + Cs^+ = Na^+ + CsX2$	3.57	3.00
$NaX3 + Cs^+ = Na^+ + CsX3$	1.64	2.10
$KX1 + Cs^+ = K^+ + CsX1$	4.76	4.50
$KX2 + Cs^+ = K^+ + CsX2$	1.44	3.77
$KX3 + Cs^+ = K^+ + CsX3$	0.95	0.70
$Ca_{0.5}X1 + Cs^+ = 0.5Ca^{2+} + CsX1$	7.53	7.13
$Ca_{0.5}X2 + Cs^+ = 0.5Ca^{2+} + CsX2$	4.55	6.46
$Ca_{0.5}X3 + Cs^+ = 0.5Ca^{2+} + CsX3$	1.44	1.58
$NaNO_3(aq) \rightarrow Na^+ + NO_3$-	0.33	0.26
$CsNO_3(aq) \rightarrow Cs^+ + NO_3$-	0.47	0.50
Bdot parameter (Cs-X)	1.66E-04	-8.90E-02
Exchange Site	**CEC (μeq g^{-1})**	**CEC (μeq g^{-1})**
Site 1	0.027	0.037
Site 2	1.43	0.14
Site 3	86.6	102

III. Key Results

Dependence of K_d on cesium and competing cation concentration

The refitting of the batch data of Zachara et al [8] confirms the strong variability of the cesium K_d for Hanford sediments. The dependence of the cesium K_d on the other cations (Na^+, K^+, and Ca^{2+}) is predicted by the ion exchange theory. We can rewrite Equation 2 to obtain an expression for the dimensionless form of the distribution coefficient, K_d':

$$K_d' = \frac{[CsX]}{[Cs^+]} = \frac{1}{K_{M/Cs}} \frac{[M_{1/m}X]}{[M]^{1/m}} \quad 4$$

It follows that cesium retardation depends on the concentration of the competing ion because cesium retardation is described by:

$$R = 1 + K_d' = 1 + \frac{\rho_B K_d}{\phi} \quad 5$$

where ρ_B is the bulk dry density of the sediment, and ϕ is the porosity. This is shown graphically by plotting the cesium K_d versus sodium concentration in solution (Figure 2a). The cesium K_d is also dependent on the cesium concentration in solution, because the different sites have different affinities for cesium exchange. If cesium concentrations in solution are close to the concentration of the high affinity frayed-edge sites, then the retardation (or K_d) for cesium will be correspondingly high. However, if cesium concentrations significantly exceed the concentration of the frayed-edge sites, the K_d will be lower because cesium uptake is dominated by the low affinity, clay surface sites. Figure 2b shows the effect of cesium concentration on the cesium K_d.

Multi-cation cesium exchange model—Batch-derived fits

Our results suggest that the Cs-Ca-Na-K exchange model derived from batch experiments predict Cs retardation in Hanford sediments in solutions with high enough Na or K concentrations to compete strongly for exchange sites. However at lower Na concentrations in the absence of an ion that strongly competes for the exchange sites, the model based on batch-fitted parameters under predicts cesium retardation by 25 to 55 percent. In Figure 3, we plot the model prediction and the experimental breakthrough curves versus the number of pore volumes to represent Cs retardation. Retardation is also listed in Table 3. In high salt solutions, 5 M $NaNO_3$, with relatively high cesium concentrations, 10^{-4} M Cs, cesium retardation is about 8 for both the model prediction and experiment. There is also a good match between model prediction and experiment in solutions containing potassium (0.1 M KNO_3, 0.9 M $NaNO_3$, and 10^{-4} M Cs), yielding a cesium retardation of about 12. However, in 1 M $NaNO_3$ solutions with no potassium, the model under predicts cesium retardation at both high and low cesium concentrations. In the 1 M $NaNO_3$ experiments, cesium retardation is 41 at 10^{-4} M Cs and 282 at 5 x 10^{-7} M Cs, compared to predicted retardation equal to 26 at 10^{-4} M Cs and 226 at 5 x 10^{-7} M.

Table 3. Comparison of cesium retardation model

Exp. No.	Inlet Salt Solution	Inlet Cs M	Observed Retardation	Model Retardation Batch Fit	Model Retardation Column Fit
1	1 M $NaNO_3$	10^{-4}	42.9	26.9	36.7
2	1 M $NaNO_3$	10^{-4}	40.3	26.4	36.6
3	5 M $NaNO_3$	10^{-4}	7.6	8.0	7.1
4	1 M NaOH	10^{-4}	38.7	32.4	42.5
5	1 M $NaNO_3$	5×10^{-7}	282.2	225.6	276
6	0.1 M KNO_3 0.9 M $NaNO_3$	10^{-4}	12.6	11.2	11.6

The variable agreement between the model predictions and experiments appears to be partly an artifact of fitting the batch data on a logarithmic scale. Our fits to the batch data on a log-log plot are visually very close (with the exception of 0.01 M Cs-Na exchange), with discrepancies on the order of 0.1 log unit or less. The global fit of the batch data slightly under predicts exchange in the 1 molal $NaNO_3$ batch experiments and slightly over predicts exchange in the 5 molal case. Although these discrepancies

are small in log space, at higher cesium exchange concentrations they translate into significant differences in the prediction of the total mass of exchange cesium and the resulting retardation in the column experiments. We evaluate this effect by weighting the batch exchange experiments at the $NaNO_3$ concentration corresponding to the conditions of the column experiment (Table 4). Weighting the data in this fashion improves the match between the observed and calculated retardation, but it does completely eliminate the discrepancies. Additionally, this approach limits the global application of the ion exchange model over a wide range of solution compositions that are required to model cesium migration beneath the Hanford tanks.

Table 4: Observed versus calculated retardation of cesium for case where background electrolyte batch exchange data was weighted by a factor of 10 over other data

Exp. No	**Inlet Salt Solution**	**Observed Retardation**	**Model Retardation** Batch fit optimized for salt concentration	**Model Retardation** Batch fit corrected for irreversible sites (see discussion below) and optimized for salt concentration
1	1 M $NaNO_3$	42.8	34.3	
2	1 M $NaNO_3$	40.3	35.5	40.5
3	5 M $NaNO_3$	7.6	8.3	
5	1 M $NaNO_3$	282	230	262
6	0.1 M KNO_3 0.9 M $NaNO_3$	12.6	11.3	

Multi-cation cesium exchange model—Column-weighted parameters

To further evaluate the ion exchange model, we modify our Cs-Na-K-Ca exchange model by fitting the selectivity coefficients and the cation exchange capacity with weighted results from our column experiments (Figure 4 and Table 2). Batch experiments are included as well in the fitting procedure because the column experiments do not cover the entire range of cation concentrations. The inclusion of the column-weighted data improves the match between predicted and observed cesium retardation in the 5 M $NaNO_3$, 1 M $NaNO_3$, and the mixed 0.1 M KNO_3 and 0.9 M $NaNO_3$ experiments. There are two significant differences between the model parameters fitted with the batch data and those fitted with the column data. One is the increase in the concentration of site 3 from 88.1 to 102 $\mu eq\ g^{-1}$. A second difference is the higher affinity for cesium over sodium on site 3 where the log K increases from 1.64 to 2.10. Both of these predict a higher overall mass of cesium on exchange sites for a given aqueous concentration of cesium and thus higher cesium retardation. Changes in the selectivity coefficients for the Cs-K and Cs-Ca exchange reactions are directly linked to the higher CEC in the column derived parameters. This reflects the non-uniqueness of the model, since the column experiments provided no new data for the Cs-K-Ca systems (in the experiment containing K, the experiment agreed with the model prediction based on the batch data). The higher CEC determined from a fit of the column experiments is supported by the CEC estimated from the pretreatment phase of the column experiments (Figure 5). The equivalent concentrations of eluted potassium, calcium, and magnesium and sodium in the pretreatment phase using 1 M $NaNO_3$ and 1 M KNO_3 in two separate column experiments equals 138 $\mu eq\ g^{-1}$. However, caution must be used in interpreting results based on the CEC alone because of the non-uniqueness of the fitting parameters—it is the combination of fitted CEC and selectivity coefficients that determine the predicted cesium retardation. Further experiments are in progress to verify whether the eluted cation masses are entirely present in exchange sites or whether the eluted masses include soluble salts dissolved during the flush.

Cesium exchange to frayed-edge sites on micas and to basal layers of expandable clay minerals

We have tested the cesium exchange model in the Cs-Na binary system at two different initial cesium concentrations (5×10^{-7} and 10^{-4} M) and two different salt concentrations (1 and 5 M $NaNO_3$). These two cesium concentrations were selected to test the ability of the model to predict cesium mobility where retardation is dominated by exchange to the less abundant, high affinity, frayed-edge sites on micas and by sorption to the abundant, lower affinity, exchange sites on expandable clay surfaces (Figure 4).

Assuming a two site model were used to fit the Cs exchange data at 1 M $NaNO_3$, this would correspond to about 90 percent of the cesium sorbed to frayed-edge sites at $Cs_0 = 5 \times 10^{-7}$ M compared to about 10 percent at $Cs_0 = 10^{-4}$ M. We find good agreement between the revised model predictions and the experiment for cesium retardation (Figure 4), indicating that this model may be applied over the range of cesium and salt concentrations present in S-SX tank wastes leaking into the vadose zone sediments.

The effect of potassium on cesium exchange in high salt solutions

Potassium will enhance the mobility of cesium because it has a higher affinity for the exchange sites on micas and clays than does either sodium or calcium. Our multi-cation exchange model predicts that where potassium equals the concentration of cesium, potassium will displace about 10% of the cesium on the exchange sites (batch parameters, Table 3). Since the tank wastes contain elevated concentrations of potassium as well as in sodium, we conducted exchange experiments in the K-Cs-Na system to further test the ion exchange model. Another source of potassium in the contaminant plume is from mica and feldspar minerals dissolution in the highly alkaline and thermally hot waste stream. Validation and improvement of the ion exchange model with ternary K-Cs-Na experiments at neutral pH are needed before it can be realistically applied to high base experiments.

Figure 4 compares cesium exchange to Hanford sediments in solutions in the ternary K-Cs-Na and the binary Cs-Na systems. Initial cesium concentration (10^{-4} M) and total salt concentration (1 M) are the same in both experiments. In salt solutions containing 0.1 M KNO_3 and 0.9 M $NaNO_3$ cesium retardation is one-third its retardation in 1 M $NaNO_3$. We see excellent agreement between the predicted breakthrough and the experimental breakthrough.

Cesium exchange in high base solutions

It is important to establish whether the multi-cation cesium exchange model can be extrapolated to high base concentrations reported in the S-SX tank farms inventory. While pH does not have a direct effect on the exchange of cesium, it can have an indirect effect through aqueous complexation. In the nitrate-dominated system considered here, the pH dependence of complexation is not an important effect because the cations do not form strong pH-dependent complexes (although there is some complexation as $NaOH_{aq}$). The high base concentrations could also result in substantial alteration of the primary mineralogy of the sediment. Mineral dissolution and precipitation reactions can effect cesium mobility by altering the number and distribution of sites and by providing a source for dissolved potassium that competes for cesium exchange. Figure 6 compares cesium breakthrough curves and associated model predictions from 1 M NaOH experiment (pH 13.7) and the 1 M $NaNO_3$ experiments (pH 8) both with $Cs_0 = 10^{-4}$ M. Cesium retardation is under predicted in the 1 M $NaNO_3$ experiments and over predicted in the 1 M NaOH experiments by about the same amount (10-15%), suggesting the model can be extended to the alkaline tank waste. This model incorporates the measured OH^- and K^+ (1.5×10^{-4} M) at steady-state, but did not explicitly account for mineral dissolution or precipitation. About 4 wt. % of the sediment dissolved based on the composition of the output solutions. During the first few hours of reaction, there is rapid dissolution and re-precipitation of the sediments. SEM images and semi-quantitative EDS analyses of the sediments at the end of the experiment reveal a precipitate that is rich in silica, iron, magnesium and calcium. This precipitate is probably amorphous, because it was not detected by XRD. It is difficult to quantify the cation exchange capacity. Isotopic ^{22}Na equilibrium determinations of the CEC at the end of the experiment varied considerably and were about one-fourth the CEC of the unreacted sediments determined by the same method. In contrast, the XRD analyses suggest that the concentration of the exchange site in the reacted and the unreacted sediments is the same, because the relative concentration of smectite (expandable clay) and mica is the same. An accurate measure of the CEC at steady-state would improve the model prediction. The concentration of dissolved potassium in the high base experiments (1.5×10^{-4} M) has a small but detectable effect, lowering slightly the cesium retardation.

Reversibility of Cesium Exchange

The cesium exchange model presented here assumes cesium exchange to the frayed-edge mica sites and to basal clay surfaces is rapid and reversible. It does not consider cesium sorption to irreversible sites. Laboratory studies show that cesium diffuses within mica microfissure, interlamellar, and collapsed frayed-edge sites effectively fixing the cesium to the solids [1-5]. More importantly, cesium does not easily desorb from contaminated sediments taken from cores near or beneath leaking S-SX tanks even

when using aggressive techniques [6]. It is important to assess the reversibility of cesium exchange, because once the sediments are contaminated they become a potential contaminant source for the underlying sediments and groundwater. Equally important is to determine the total mass of cesium incorporated into irreversible exchange sites.

Figure 7 shows the cesium sorbed and desorbed versus pore volume for three experiments, 10^{-4} M Cs and 5 M $NaNO_3$, 5 x 10^{-7} M Cs and 1 M $NaNO_3$, and 10^{-4} M Cs and 1 M NaOH., as well as their respective model predictions based on the column parameters. In our reactive transport experiments cesium exchange is reversible only in experiments where cesium and competing salt concentrations are high. In the 10^{-4} M Cs and 5 M $NaNO_3$ experiment, 98% of the cesium that was taken up by the sediments was desorbed when flushed with 5 M $NaNO_3$. This is expected at these high cesium and salt concentrations because cesium sorption is dominated by exchange to basal sites in the expandable clays. At lower cesium and salt concentrations, however, cesium sorption is dominated by exchange at high affinity, frayed-edge mica sites, which may exhibit irreversible behavior. In the experiment using 5 x 10^{-7} M Cs and 1 M $NaNO_3$ experiment approximately 70% of the cesium was desorbed by a flush of 1 M $NaNO_3$ following the cesium sorption phase. As indicated by equilibrium modeling of this experiment, most of the mass of cesium remaining on exchange sites at the end of experiment remains there because of the high affinity of these sites for cesium, not because of any irreversibility associated with these sites. The high affinity of these sites for cesium means that many pore volumes are required to completely desorb all cesium. There is some evidence, however, for irreversibility as indicated by the discrepancy between the equilibrium modeling results and the observed cesium concentrations. This is best shown in the 5 x 10^{-7} M Cs and 1 M $NaNO_3$ experiment. During the sorption phase of the experiment between 282 and 617 pore volumes, the lower cesium concentrations in the effluent compared to the model results may indicate that some cesium is incorporated irreversibly into exchange sites. Similarly, during the desorption phase, the observed cesium concentrations are higher than those predicted by the equilibrium modeling, indicating slow desorption of cesium.

The discrepancy between the equilibrium modeling and observed results can be used to assess the concentration of irreversible cesium exchange sites. During the sorption stage between 282 and 617 pore volumes, the discrepancy between the equilibrium model and observed results indicates irreversible sorption of 7.5 x 10^{-6} moles total cesium or 4.4 x 10^{-7} mol Cs/g sediment. On the desorption limb, the discrepancy corresponds to 9.5 x 10^{-6} moles total cesium or 3.5 x 10^{-7} mol Cs/g sediment. In experiment 2 carried out with 10^{-4} M cesium, the discrepancy during the sorption phase corresponds to 4 x 10^{-4} moles total cesium or 1.9 x 10^{-5} mol Cs/g sediment. These masses of cesium associated with irreversible sites are minimum values, since any irreversible sorption occurring prior to the breakthrough of cesium cannot be detected with this method.

In the high base experiment using 1 M NaOH, however, the relatively high cesium concentrations of 10^{-4} M suggest that exchange should be primarily on reversible clay sites. However, only about 72% of the cesium desorbs by a flush of 1 M NaOH. Unlike the 5 x 10^{-7} M and 1 M $NaNO_3$ experiment which exhibited a constant release of cesium during the last half to the experiment, the release of cesium approaches zero in the outflow solution in the 1 M NaOH experiment. The fact that 28% of the cesium remains tied up in the sediments suggests that exchange substrates have been altered by the high base solution. This observation may explain why cesium does not easily sorb from the contaminated Hanford sediments [6].

We have established that some of the discrepancy between the batch-based ion exchange model and the experimental column data may reflect the cesium incorporated into irreversible sites. If cesium sorbs to the irreversible sites prior to the initial breakthrough ($C/C_0 = 0.5$), it would show up simply as delay in the observed retardation compared to the predicted retardation, because the irreversible sites are not included in the model. In this analysis we apply "corrections" for sorption to irreversible sites to the retardation predicted with the batch-derived parameters optimized for the salt concentration of the column experiments (comparison of retardation is shown in Table 4). Using the discrepancy between the equilibrium model and the observed results for the 5 x 10^{-7} M Cs and 1 M $NaNO_3$ experiment (Experiment 5), we calculate an average rate of cesium sorption to these sites equal to 4.9 x 10^{-8} mol/hour from 282 to 617 pore volumes. Application of this rate of irreversible cesium sorption prior to the initial breakthrough of cesium ($C/C_0 = 0.5$) would increase the predicted breakthrough time from 230 to about 262 pore volumes. This retardation value is within 7% the experimental retardation of 282 pore volumes (Table 4). We apply the same analysis to Experiment 2 where the aqueous cesium concentration is higher, 10^{-4} M Cs. In this case, we calculate an average rate of cesium exchange at these sites equal to 1.3 x 10^{-5} mol /hour.

When this "correction" is applied the predicted retardation shifts to about 40.5, in agreement with the experimental value (Table 4). Note that this interpretation of the batch-column discrepancy relies on an irreversible chemical process as opposed to diffusion-controlled transport into immobile zones within the sediment. A rate-limited process based on diffusion through porous media would have no effect in a batch system where stirring makes the sediment material fully accessible to the bulk solution.

Additional evidence for irreversible cesium exchange may be seen in the comparison of the breakthrough curves of 10^{-4} M Cs and 1 M $NaNO_3$ experiments run at two different flow rates. In Experiment 1 run at 0.02 ml/min the retardation is slightly greater (R= 43) than the retardation of in Experiment 2 run at 0.1 ml/min (R=40). The slightly higher retardation at flow rates that are five times slower may indicated more cesium has had time to diffuse into the irreversible sites. Note also, that Experiment 1 run at a slower flow rate and over a longer period of time than Experiment 2 shows less undershooting of the equilibrium model results than does Experiment 2. Once again, this is consistent with longer reaction time for cesium diffusion to the irreversible sites, where the discrepancy between the equilibrium model and the experiment would be manifest in a delayed retardation and not in a mismatch between the prediction and experiment at $C/C_0 > 0.5$. Finally, Experiment 5, which was designed to increase the relative importance of the FES versus clay sites by using a lower cesium concentration, shows stronger irreversible effects than any other experiments. This may be an argument that the rate-limited behavior demonstrated by cesium may be due to irreversible chemical processes rather than to a rate limitation based on transport rates.

IV. Implications

One of the most significant implications of this work is the confirmation that the ^{137}Cs distribution coefficient is not constant over the range of sodium, potassium, (calcium) and cesium concentrations found in the tank farm inventory and in the vadose zone pore water at Hanford. Vadose zone processes, such as dilution from infiltrating rain water (or water leaking from pipes) or concentration from boiling waste, will dramatically alter the ^{137}Cs K_d over time and space. Moreover, a ^{137}Cs K_d determined directly from the contaminated sediments is suspect unless proper adjustments are made, because those determinations typically involve dilutions as part of the analytical procedure. A 10X dilution, for example, could easily result in overestimating the K_d by a factor of 3 to 10. Similar cautions apply even when no dilutions for analytical purposes are carried out, because infiltration of rainwater in the vadose zone is likely to have diluted cation concentrations from what they were at the time of the leak. It is quite probable, that a K_d determined from present day contaminated sediments might significantly overestimate the cesium retardation at the time of the tank leaks.

The multi-cation exchange model captures much of the chemical effects responsible for the dependence of ^{137}Cs K_d on competing cation and cesium concentrations, and is a significant improvement over the use of a constant K_d to model ^{137}Cs form tank leaks to the vadose zone sediments. However, there is some mismatch between the predictions derived from a global fit of batch data covering a wide range of cesium and salt concentrations and our 1-D column experiments. Part of the mismatch appears to be related to the sorption of cesium at irreversible sites, which has not yet been included in the modeling. Additional experimental data would be needed to better quantify these sites as well as the cation exchange capacity. In the absence of these new experimental data, model parameters based on weighted column experiments can be used in field-scale analyses of transport to provide a more direct measure of retardation of cesium in Hanford sediments.

The following example shows that the multi-cation exchange model describes ^{137}Cs retardation that is consistent with ^{137}Cs observations at the SX tank farm. Our column experiments indicate that high competing cation concentrations associated either with the tank liquors or resulting from reactions in the sediment underlying the tank cause a significant decrease in the retardation of cesium. The SX-115 tank leak apparently contained about 3.5 M $NaNO_3$ and 8 x 10^{-5} M Cs. Our model for cesium migration suggests a dimensionless cesium K_d of about 10 prior to any dilution of the tank liquors by vadose zone processes. This qualitatively agrees with the strong retardation of cesium observed below SX-115. In addition, some retardation of sodium is expected upon dilution of the leaked waste, again in agreement with observations made in bore hole WB 23-19 [7]. In contrast, leaking tank liquors at SX-108 were at or above the boiling temperature and were extremely concentrated, with some estimates giving $NaNO_3$ concentrations at or close to equilibrium with respect to solid $NaNO_3$ (about 19.5 molal at 100°C) and 7 x 10^{-4} M Cs.. At these very high $NaNO_3$ concentrations, one does not expect to see any retardation of sodium, in agreement with field observations, which show that sodium peaks are coincident with nitrate

peaks. One also expects significantly less retardation of cesium as well. Extrapolating the column-weighted fits of cesium exchange to 15 M yields a predicted cesium retardation of between 2 and 3. This value is close to the observed retardation below SX-108 of 2.5 to 3 [7]. While this prediction is uncertain until we have direct experimental confirmation of cesium retardation at these $NaNO_3$ concentrations and at higher temperature, the ion exchange model presented here suggests that the high salt concentrations account for the bulk of the enhanced cesium mobility observed, particularly below the SX-108 tank.

An important aspect of the present study has been to provide additional scientific justification for the ion exchange model proposed by Zachara et al [8] to describe cesium migration in Hanford sediments. We believe the combination of reactive transport modeling and column flow-through experiments provide very strong support for the applicability of the ion exchange model. As summarized above, our results suggest that the bulk of the enhanced migration of cesium observed below tanks like SX-108 is the result of the very high salt concentrations in these tanks. Tanks with lower salt concentrations thank SX-108 show correspondingly higher cesium retardation. The multi-site ion exchange model also suggests that relatively dilute fluids of the kind associated with natural infiltration are unlikely to mobilize cesium in the subsurface. The ion exchange model, however, does suggest that considerable caution should be used in designing any sluicing methods, since re-injection of a concentrated sluicing solution is likely to result in further cesium migration.

References

1. Lomenick, T.F., Tamura, T., *Naturally occurring fixation of cesium-137 on sediments of lacustrine origin.* Soil Sci. Soc. Proc. Amer, 1965. **29**: p. 383-387.
2. Klobe, W.D., Gast, R. G., *Conditions affecting cesium fixation and sodium entrapment in hydrobiotite and vermiculite.* Soil Sci. Soc. Amer. Proc., 1970. **34**: p. 746-750.
3. Le Roux, J., Rich, C. I., Ribbe, P. H., *Ion selectivity by weathered micas as determined by microprobe analysis.* Clays Clay Miner., 1970. **18**: p. 333-338.
4. Comans, R.N.J., Haller, M. DePreter, P., *Sorption of cesium on illite: Non-equilibrium behavior and reversibility.* Geochim. Cosmochim. Acta, 1991. **55**: p. 433-440.
5. Smith, J.T., Comans, R. N. J., *Modeling the diffusive transport and remobilization of 137-Cs in sediments: The effects of sorption kinetics and reversibility.* Geochim. Cosmochim. Acta, 1996. **60**: p. 995-1004.
6. McKinley, J.P., Serne, R. J., Zachara, J. M., Zeissler, C. J., Lindstrom, R. M., *The distribution and retention of 137-Cs in sediments beneath leaked waste at the Hanford site.* Environmental Science and Technology, 2001. **submitted**.
7. Serne, J., *Need references for Serne's work on Hanford bore hole geochemistry.*, . 2001.
8. Zachara, S., Liu, McKinley, Serne, Gassman, *Sorption of Cs+ to micaceous subsurface sediments from the Hanford Site, USA.* Geochim. Cosmochim. Acta, 2001. **submitted**.
9. Steefel, C.I., Yabusaki, S. B., *OS3D/GIMRT: software for modeling multicomponent-multidimensional reactive transport.* 1 ed. User's Manual and Programmer's Guide. 2001: in press, LLNL.
10. Appelo, C.A.J., Postma, D., *Geochemistry, groundwater and pollution.* 1996, Rotterdam: A. A. Balkema.
11. Felmy, A.R., *GMIN, A Computerized Chemical Equilibrium Program Using a Constrained Minimization of the Gibbs Free Energy: Summary Report*, in *Chemical Equilibrium and Reaction Models*. 1995, Soil Science Society of America: Madison, Wisconsin.

This work was performed under the auspices of the U.S. Department of Energy by the University of California, Lawrence Livermore National Laboratory under Contract No. W-7405-Eng-48.

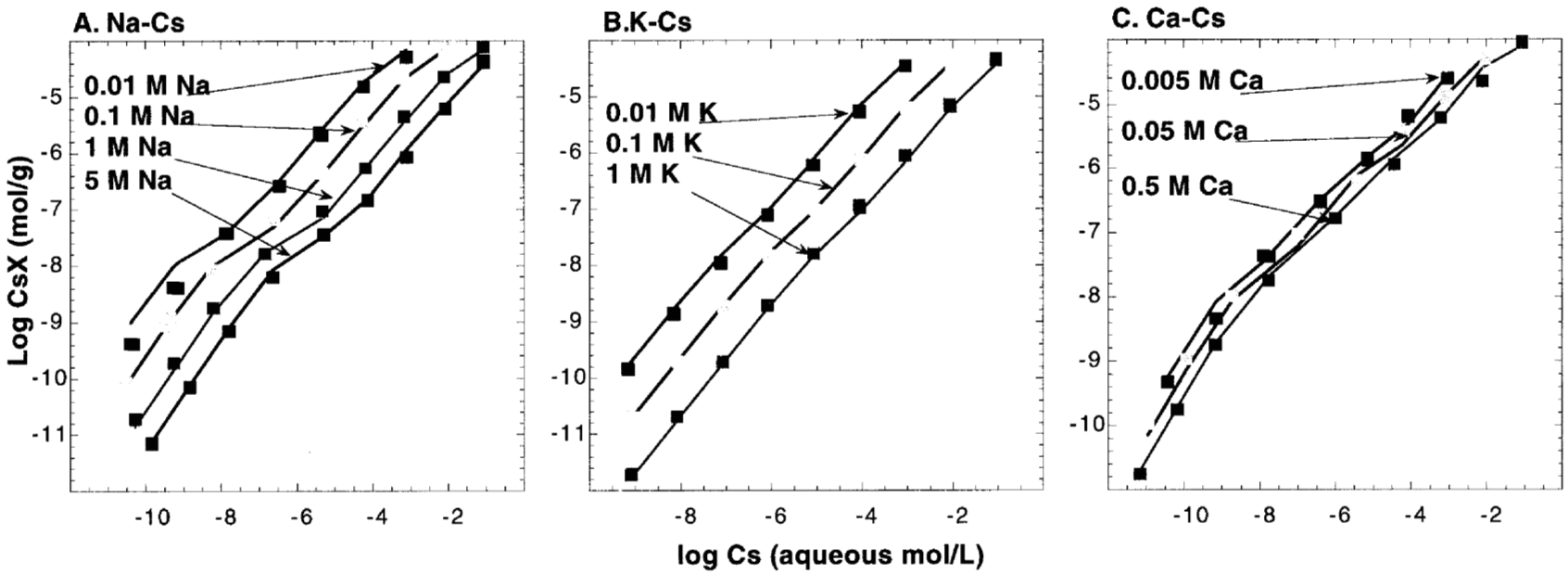

Figure 1. Comparison of cesium exchange to Hanford sediments measure in binary batch experiments (symbols) with multi-cation exchange model (solid lines) with selectivity coefficients and exchange sites derived from a global fit to all of the binary data shown in this figure. Batch data are from Zachara et al (2001).

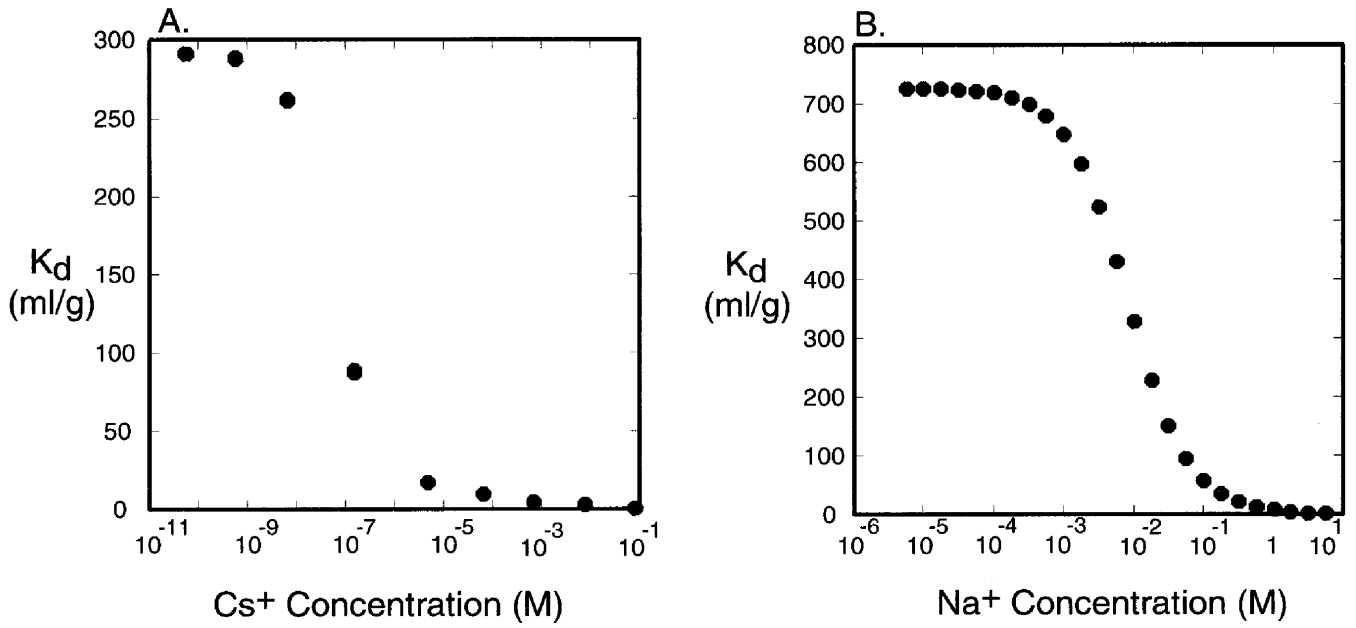

Figure 2. The dependence of cesium K_d on dissolved cesium (A) and sodium (B) concentrations calculated with the multi-cation exchange model.

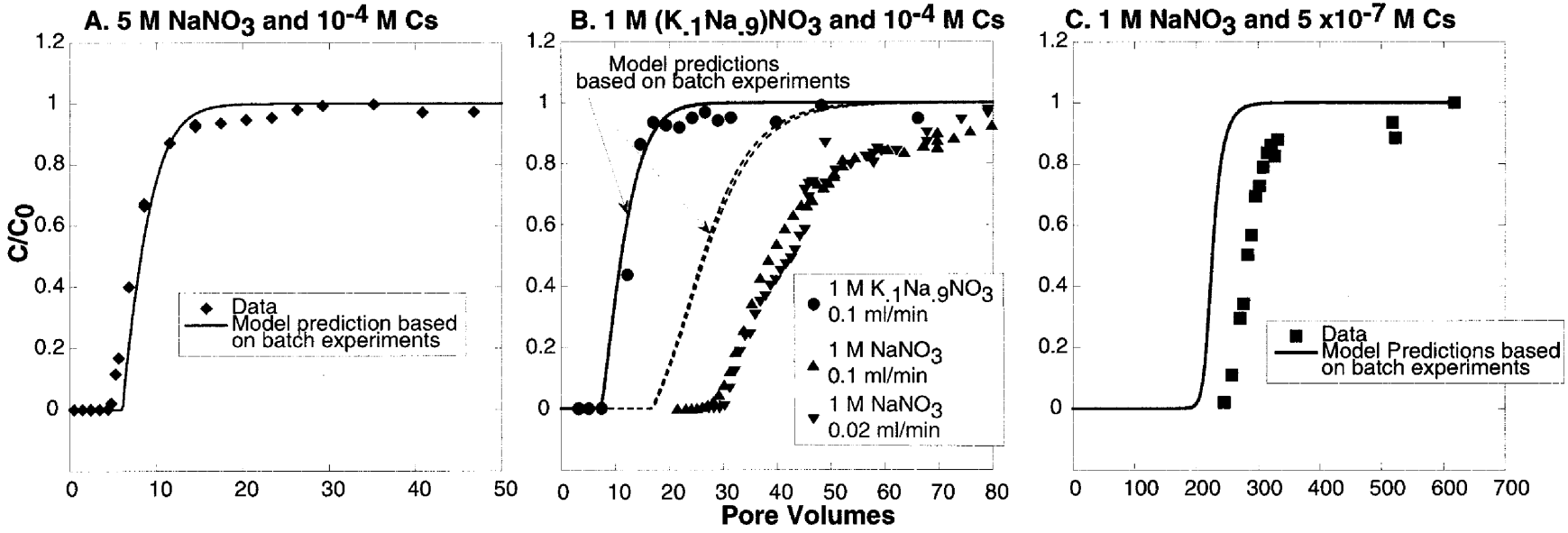

Figure 3. Cesium reactive transport through Hanford sediments in $NaNO_3$ and mixed $(K,Na)NO_3$ solutions. Comparison of cesium breakthrough curves predicted by the multi-cation exchange model derived from batch experiments (lines) with experiments (symbols).

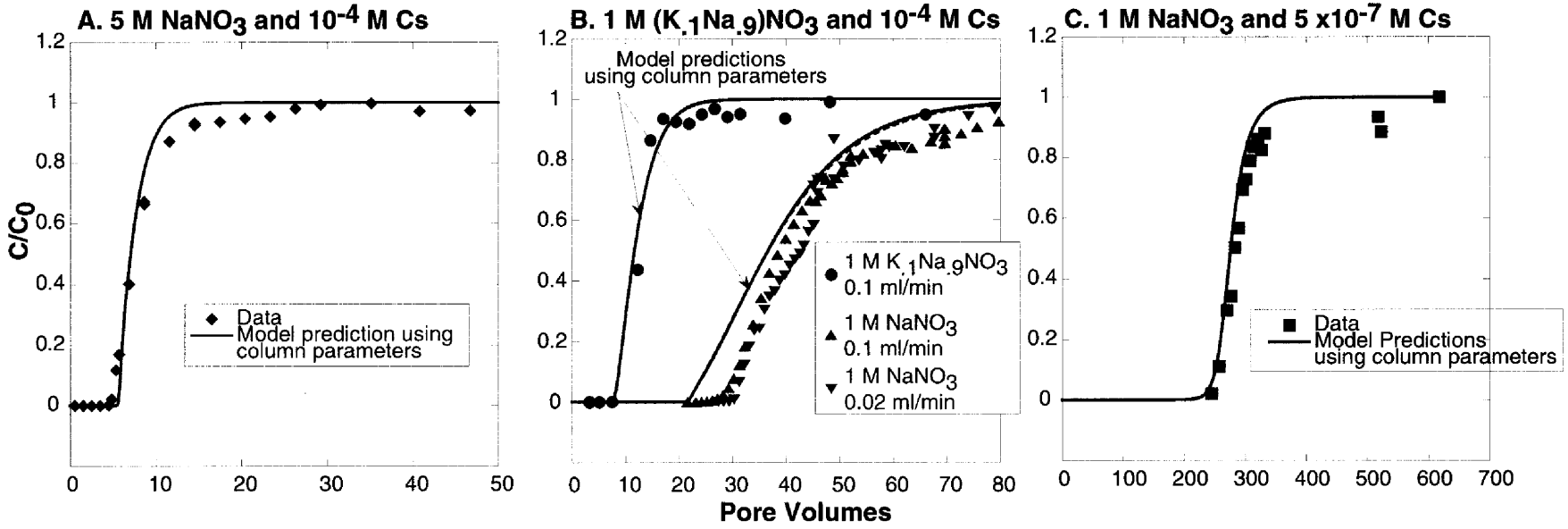

Figure 4. Cesium reactive transport through Hanford sediments in $NaNO_3$ and mixed $(K,Na)NO_3$ solutions. Comparison of cesium breakthrough curves predicted by the multi-cation exchange model derived from fits weighted to the column experiments (lines) with experiments (symbols).

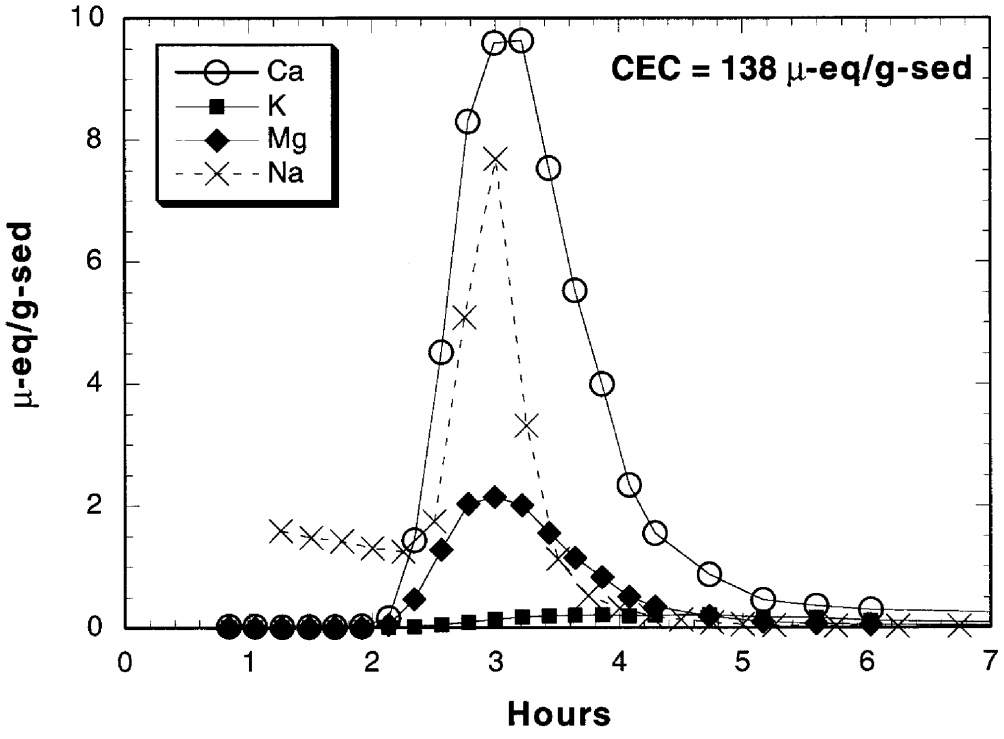

Figure 5. The cation exchange capacity measured from the equivalent concentration of Ca, K, Mg, exchanged for Na in 1 M $NaNO_3$ flushes of the sediment column, and Na exchange for K in 1 M KNO_3 flushes of the sediment column. The $NaNO_3$ and KNO_3 flushes were conducted in separate experiments with fresh sediments.

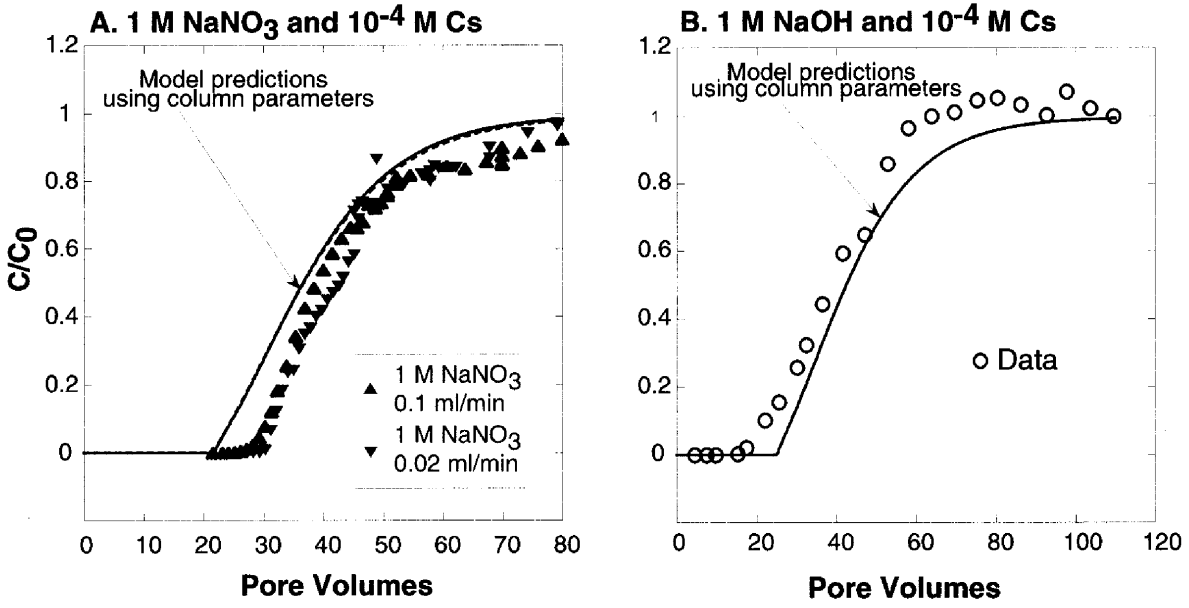

Figure 6. Comparison of cesium reactive transport through Hanford sediments in 1 M$NaNO_3$ and 1M NaOH solutions. Cesium breakthrough curves predicted by the multi-cation exchange model derived from fits weighted to the column experiments are shown by lines. The experimental data is shown by symbols.

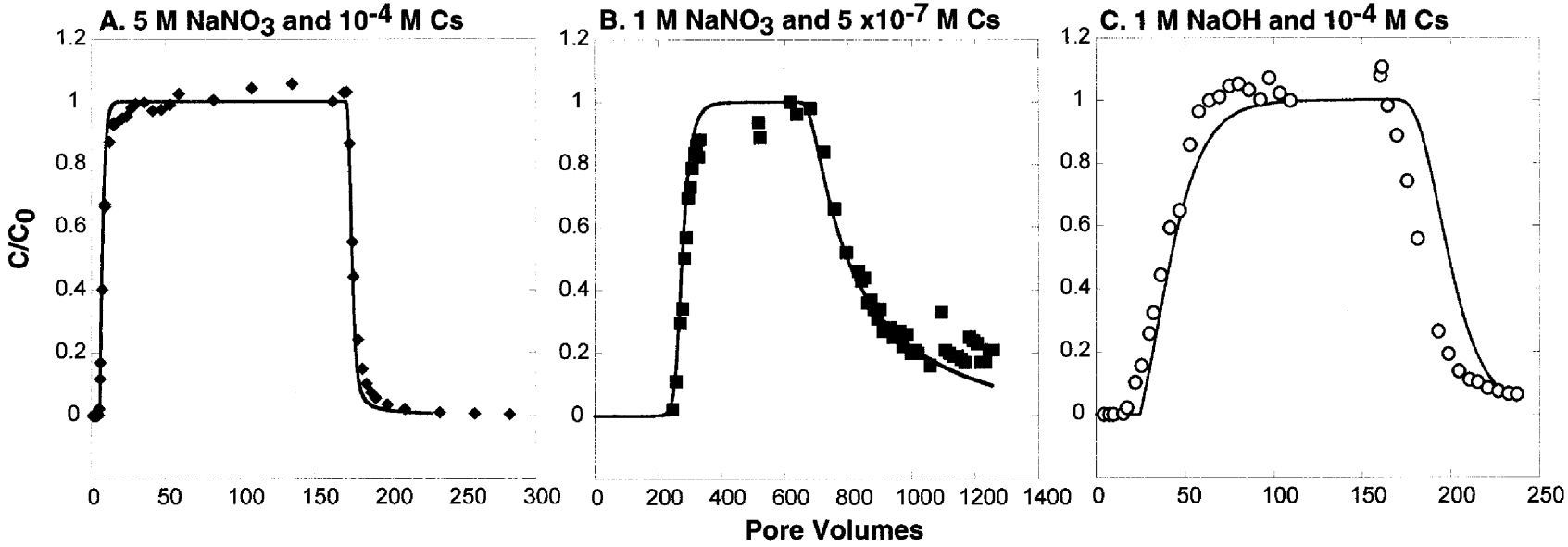

Figure 7. Reversibility of cesium exchange when flushing the sediments with 5 M NaNO3 (A), 1 M NaNO3 (B) and 1 M NaOH (C) solutions at the end of the sorption experiments. Experimental data are shown with the symbols. Model predictions using the column parameters are shown with the lines.